

11. Holman, M. in *Proc. 27th Symp. on Celestial Mechanics* (eds Kinoshita, H. & Nakai, H.) 116–136 (Nat. Astron. Observatory of Japan, Tokyo, 1995).
12. Roy, A. E. *Orbital Motion* (Hilger, Bristol, 1988).
13. Levison, H. F. & Duncan, M. J. The long-term dynamical behavior of short-period comets. *Icarus* **108**, 18–36 (1994).
14. Dones, L., Levison, H. F. & Duncan, M. *Completing the Inventory of the Solar System* (eds Rettig, T. W. & Hahn, J. M.) 233–244 (ASP Conf. Proc., Astron. Soc. Pacif., San Francisco, 1996).
15. Stern, S. A. Collision timescales in the Kuiper disk: model estimates and their implications. *Astron. J.* **110**, 856–868 (1995).
16. Davis, D. R. & Farinella, P. Collisional evolution of Edgeworth–Kuiper belt objects. *Icarus* **125**, 50–60 (1997).
17. Fernandez, J. A. & Ip, W. H. Some dynamical aspects of the accretion of Uranus and Neptune: the exchange of orbital angular momentum with planetesimals. *Icarus* **58**, 109–120 (1984).
18. Malhotra, R. The origin of Pluto's peculiar orbit. *Nature* **365**, 819–821 (1993).
19. Malhotra, R. The origin of Pluto's orbit: implications for the solar system beyond Neptune. *Astron. J.* **110**, 420–429 (1995).
20. Morbidelli, A. & Valsecchi, G. B. Neptune scattered planetesimals could have sculpted the primordial Edgeworth–Kuiper belt. *Icarus* (in the press).
21. Duncan, M. J., Levison, H. F. & Budd, S. M. The dynamical structure of the Kuiper belt. *Astron. J.* **110**, 3073–3081 (1996).
22. Tremaine, S. in *Baryonic Dark Matter* (eds Lynden-Bell, D. & Gilmore, G.) 37–65 (Kluwer, Boston, 1990).
23. Kowal, C. T. A solar system survey. *Icarus* **77**, 118–123 (1989).
24. Weissman, P. R. & Levison, H. F. The size distribution of cometary nuclei. *Lunar Planet. Sci.* **27**, 1409 (1996).
25. Kresak, L. Mass content and mass distribution of the asteroid system. *Bull. Astron. Inst. Czech.* **28**, 65–82 (1977).
26. Morrison, D. Asteroid sizes and albedos. *Icarus* **31**, 185–220 (1977).

Acknowledgements. I thank N. Murray and S. Tremaine for discussions, S. Dermott and H. Levison for reviews of the manuscript, and J. Wisdom for computer time for the simulations.

Correspondence should be addressed to M.H. (e-mail: holman@cita.utoronto.ca).

Cluster-derived structures and conductance fluctuations in nanowires

R. N. Barnett & Uzi Landman

School of Physics, Georgia Institute of Technology, Atlanta, Georgia 30332, USA

Understanding the variation of a material's properties with size, form of aggregation and dimensionality is becoming important in the face of increasing miniaturization of electronic and mechanical devices. Experimental studies have focused on the preparation and characterization of solid-state nanometre-scale structures such as metal and semiconductor nanocrystals^{1–3}, surface-supported structures and quantum dots⁴ and nanoscale junctions or wires^{5–22}. It has emerged that these nanostructures can often be fruitfully described using concepts and methodologies developed in the contexts of gas-phase atomic clusters and atomic nuclei^{23–25}. Here we make this connection explicitly through first-principle molecular dynamics simulations^{22,26} which show that, as nanowires of sodium metal are stretched to just a few atoms in diameter, the structures formed by metal atoms in the neck can be described in terms of those observed in small gas-phase sodium clusters²⁷. We find that the electronic spectral and conductance characteristics of these atomic-scale contacts exhibit dynamical thermal fluctuations on a sub-picosecond timescale, owing to rearrangements of the metal atoms, which will significantly affect the transport properties of such nanowires.

Formation and mechanical properties of interfacial junctions (in the form of nanowires) have been predicted through early molecular dynamics simulations⁵, where the materials were modelled using semiempirical embedded-atom potentials. In these studies it was shown that separation of the contact between materials leads to generation of a connective junction which elongates and narrows through a sequence of structural instabilities; at the early stages elongation of the junction involves multiple slip events, whereas at the later stages, when the lateral dimension of the wire narrows to a diameter of ~ 15 Å, further elongation involves a succession of stress accumulation and fast relief stages associated with a

sequence of order–disorder structural transformations localized to the neck region^{5,19,20}. These predictions, as well as anticipated electronic conductance properties^{5,6} have been corroborated in a number of experiments using scanning tunnelling and force microscopy^{5,7–9,11,16,21}, break junctions¹⁰ and pin–plate techniques^{13,19} in ambient environments, as well as under ultra-high vacuum and/or cryogenic conditions.

One of the most fascinating aspects of such nanowires is the prospect of formation of atomic-scale contacts and switches^{5,11,14,18} which may occur towards the ultimate stages of elongation (that is before complete physical separation, or breaking, of the wire). Understanding the atomic rearrangements and structural evolution, electronic properties, and dynamics of such nanojunctions, particularly as they approach the ‘one-atom contact’ regime, is a significant challenge requiring a detailed theoretical description based on first-principles electronic structure calculations. To this end we have used the Born–Oppenheimer (BO) local-spin-density (LSD) molecular dynamics (MD) method (for details of the BO–LSD–MD, see ref. 26) for sodium wires, where the dynamics of the ions (with an integration time-step of 3 fs) evolves at finite temperature ($T = 190$ K) on concurrently calculated ground-state potential-energy surfaces, evaluated self-consistently for each ionic configuration using the LSD theory, in conjunction with non-local norm-conserving pseudopotentials²⁸ with a 6.2 Ry plane-wave energy cut-off.

The simulation starts from a sodium block of bulk body-centred cubic (b.c.c.) (100) layers oriented along the z -axis and tapered to a narrowing in the middle. The periodic super-cell with (x,y,z) dimensions (19.98 Å, 19.98 Å, 21.3 Å) contains a total of 119 atoms treated dynamically, supported at the top and bottom by static (100) layers (25 atoms each); one of these layers is in the cell and the other is its periodic image. After equilibration the structure of the junction is mostly b.c.c., except in the middle layer (Fig. 1a). Each subsequent elongation involves a uniform dilation in the z direction, followed by steepest-descent energy minimization and dynamical equilibration for several picoseconds (at the start of the equilibration period stochastic thermalization to 190 K is used).

The atomic configurations of the sodium wire at selected stages of elongation shown in Fig. 1 reveal development of cluster-derived structures at the narrow-neck region. Particularly striking is the formation of a 13-atom (slightly distorted) icosahedron (5-fold symmetric), supported between the upper and lower parts of the wire (Fig. 1b,c); this structure may also be viewed as two Na₇ pentagonal bipyramidal clusters sharing an apex atom. Subsequent elongation results in ‘opening’ of the structure (Fig. 1d), and stretching of the contact past this stage results in formation of a pentagonal bipyramidal Na₇ cluster (top) bonded through one of its apex atoms to the upper atom of a tetrahedral cluster (bottom), giving the appearance of a stretched sodium dimer at the narrowing (Fig. 1e). Further elongation results in breaking of the nanowire (Fig. 1f). The occurrence of these molecular-like supported structures, which correlate with those derived for isolated sodium clusters²⁷, suggests that in atomic-scale narrow contacts the atomic coordination and nature of bonding may be described using information from investigations pertaining to small (isolated) clusters. In a certain sense the reduced dimensions, increased surface-to-volume ratio, and atomically impoverished environment in such nanoscale solid-state junctions provide a link to the realm of finite-size cluster science, where ground-state (and isomeric) structures are different from the bulk, and ‘magic numbers’ are known to occur^{23–25,27}. (Here ‘magic numbers’ refers to the enhanced stability of certain sequences of cluster sizes, shapes and structural motifs due to electronic and/or geometric-packing shell effects, which may vary from one class of materials to another.)

Contour plots of the self-consistent local effective potential confining the electrons to the wire are shown in Fig. 2 for the 23.97-Å and 29.96-Å wire configurations (compare Fig. 1b and e).

These confinement potential profiles outline the shape of the wire; we note the rather ‘smooth’ appearance of the ‘effective potential tube’ (defined by the peripheral outermost solid contour corresponding to the Fermi energy), as a result of effective screening; the approach of the confining potentials to the vacuum level (beyond the outer dashed contour) is similar for both wires, indicating a reduced screening in the more elongated one. In this context we note the close-to-circular shapes of the confining potentials at the narrowing (particularly as the wire narrows; see right-hand panels in Fig. 2), which correlates with the conductance quantization pattern⁶ reported for sodium wires¹⁰.

We now examine the electronic spectral properties of these nanowires, and their transport characteristics. The time-averaged global and local (in the narrowing) electronic densities of states (DOS), obtained from a dynamical simulation at 190 K of the

nanowire corresponding to the selected configuration shown in Fig. 1b, is displayed in Fig. 3a, along with the time-variation of the DOS at the Fermi level, $N(\epsilon_F)$ in Fig. 3b). We observe that while both the global and local $N(\epsilon_F)$ are finite, indicating metallic character, they exhibit significant fluctuations on a subpicosecond timescale (Fig. 3b), originating from redistribution of the electronic energy levels caused by ionic motion. Such fluctuations are expected to be portrayed in the electronic transport through the nanowire.

Using the density-functional Kohn–Sham orbitals the electronic conductivity, $\sigma(\omega)$, can be calculated from the linear-response (Kubo) formula^{29,30}

$$\sigma(\omega) = \frac{2\pi e^2 \hbar}{\Omega m} \sum_{ij} \frac{(f_i - f_j)}{\epsilon_i - \epsilon_j} \left| \langle i | \hat{p}_z | j \rangle \right|^2 \delta(\epsilon_i - \epsilon_j - \hbar\omega) \quad (1)$$

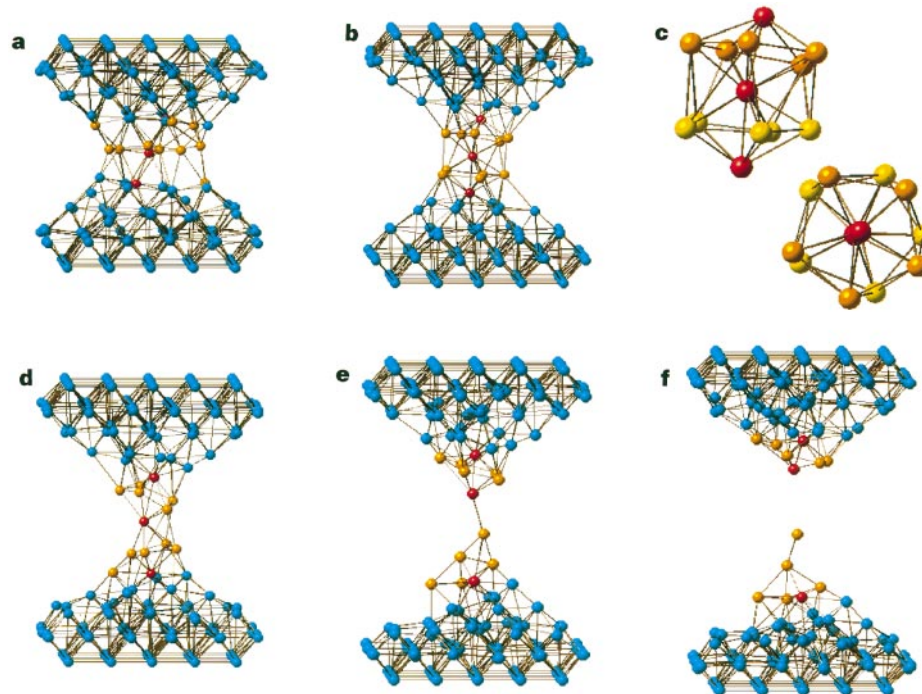


Figure 1 Atomic configurations of a sodium nanowire at selected elongation stages, obtained through first-principles molecular dynamics simulations. The configurations in **a**, **b**, **d**, **e** and **f** correspond to wires of lengths 21.3 Å, 23.97 Å, 26.64 Å, 29.96 Å and 31.96 Å, respectively. In **c**, side and top views are shown of the stretched icosahedral supported cluster (see neck region in **b**). The 13 atoms forming the icosahedron are distinguished also by colour in the other configurations to allow visualization of the structural evolution.

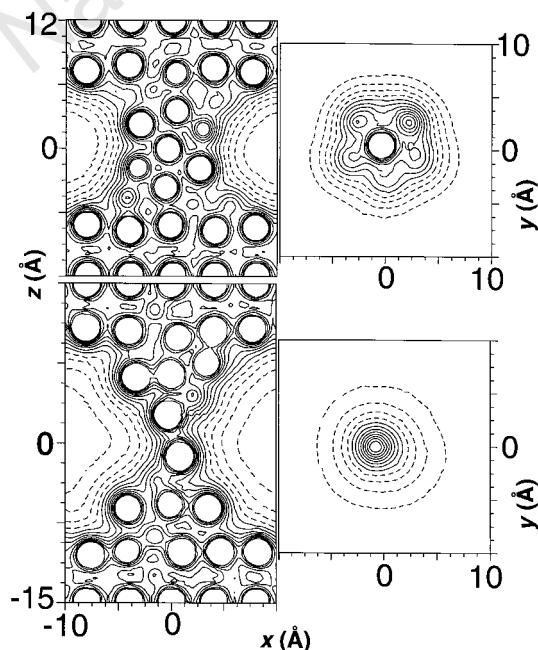


Figure 2 Contour plots of the local part of the self-consistent LSD effective potentials corresponding to the wire configurations shown in Fig. 1b (top panel) and Fig. 1e (bottom panel); contours inside the repulsive atomic cores, where the non-local contribution is significant, are not shown. On the left, contours are in the plane containing the axis (z) of the wire; on the right they are drawn in the transverse plane at the narrowest part of the wire. All contours, with a spacing of 0.68 eV, correspond to energies below the vacuum level, with the solid lines corresponding to energies below ϵ_F ; from the difference between the vacuum level and ϵ_F the work function of the wires is estimated as ~ 2.1 eV.

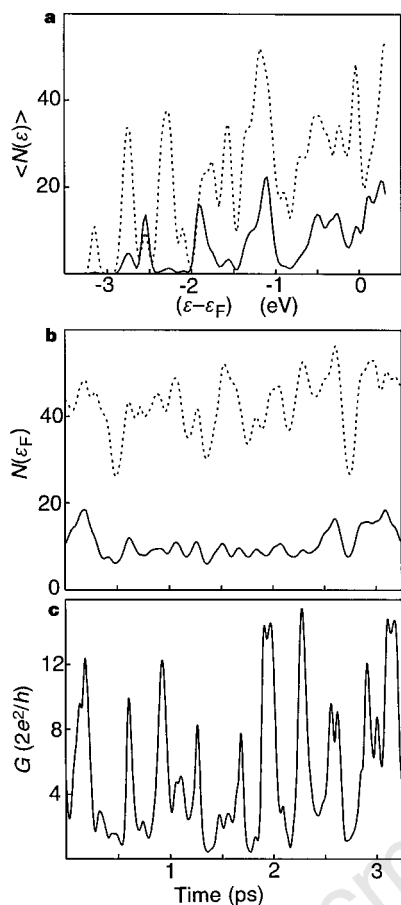


Figure 3 Spectral and conductance characteristics for the 23.97-Å nanowire (Fig. 1b). **a**, Time averages (from simulations at 190 K) of the global (dashed line) and local (solid line; evaluated at the narrowest, cluster, region) densities of states, $\langle N(\epsilon) \rangle$. **b**, Time variations of the global and local DOS at ϵ_F . **c**, Time variation of the conductance G , showing sub-picosecond fluctuations, with an average value of $(5.2 \pm 0.7)g_0$. The Kubo conductivity formula (equation (1), main text) used in our calculations has been discussed previously^{23,30} and its use in conjunction with finite-temperature simulations alleviates to a large extent some of the issues discussed there. In our calculations the delta-function is represented by a gaussian with a width of $\eta = 0.0163$ eV ($\eta/k_B = 190$ K), which is equal to half the average level spacings near ϵ_F . Larger broadening decreases, but does not obliterate, the magnitude of the conductance fluctuations.

where m is the electron mass, f_i is the occupation (Fermi function) for the LSD Kohn–Sham level of energy ϵ_i , $\hat{p}_z = -i\hbar\partial/\partial z$, and Ω is the volume of the periodic calculational cell ($\Omega = AL$, where A and L are, respectively, the periodic-cell transverse area, and length along the nanowire axis). Extrapolation of the time-averaged conductance $\langle G(\omega) \rangle = \langle \sigma(\omega) \rangle A/L$ to $\omega \rightarrow 0$, yields for the 23.96-Å nanowire a d.c. conductance $\langle G \rangle = (5.2 \pm 0.7)g_0$, where $g_0 = 2e^2/h$ ($g_0^{-1} = 12.9$ k Ω) and the statistical error is estimated following ref. 31. Similar analyses yield conductance values of $(11.0 \pm 1.5)g_0$ and $(1.2 \pm 0.3)g_0$ respectively for the 21.3-Å and 26.64-Å wires (Fig. 1a and d); for the 29.96-Å wire (Fig. 1e), a value much smaller than $1g_0$ is predicted (a similar structure and conductance were obtained also for a 28.1-Å wire). The conductance shows an expected decreasing trend as the wire narrows; we note here that no attempt has been made here to search for wire configurations (that is elongations) that may yield a particular sequence of conductance values. These results, as well as the lateral shapes of the effective confinement at the narrowing (Fig. 2) may be compared with phenomenological quantum and semi-classical theories of electronic conductance in wires.^{6,15,17–20,32} In such theories, the confinement of the nano-

constriction is often modelled using hard-wall potentials (or variations thereof, including finite height of the confining potential and electron density spill-out effects), and the conductance channels (in the framework of a Landauer theory) are determined as the lateral electronic states (including their degeneracies) calculated at the narrowest part of the constriction. Our calculated average conductance values are in good correspondence with such semi-classical estimates (except for the lowest one where such estimates are not reliable¹⁵). For example, using the Weyl-modified Sharvin formula corrected for the finite height of the confining potential (equation (3) in ref. 15, with $\alpha = 0.1$ and $k_F = 0.92 \text{ \AA}^{-1}$) gives a value of $5.2g_0$ for a cylindrical wire with a cross-sectional radius of 5.2 Å. This compares favourably with an effective radius of 4.9 Å determined from the confining potential contour (at ϵ_F) corresponding to the 23.97-Å wire (see upper-right cross-sectional view in Fig. 2) for which, as described above, we obtain through equation (1) $\langle G \rangle = (5.2 \pm 0.7)g_0$.

In light of our above-mentioned observation of temporal fluctuations in $N(\epsilon_F)$, caused by finite-temperature dynamical structural fluctuations, we show in Fig. 3c the corresponding calculated time variations of G (whose time-average yields the value of $5.2g_0$). The resonance-like features in G correlate with the temporal structural and electronic spectral fluctuations (in both the local density of states and momentum matrix elements) due to thermal vibrations. Such finite-temperature effects and factors related to the ‘non-ideal’ (structural) nature of the nanowires underlying scattering of the electrons, as well as inherent irreproducibility in the fabrication of the nanowires through contact elongation or break junction techniques, are likely to be the sources of the distribution of measured conductance values (commonly displayed as conductance histograms of G). Consequently, our results suggest that dynamical conductance fluctuations may be of importance in considerations pertaining to atomic-scale contacts, and that they might be identified experimentally by fast spectroscopical measurements of electronic transport in nanowires. □

Received 13 February; accepted 6 May 1997.

- Whetten, R. L. *et al.* Nanocrystal gold molecules. *Adv. Mater.* **8**, 428–433 (1996).
- Luedtke, W. D. & Landman, U. Structure, dynamics and thermodynamics of passivated gold nanocrystallites and their assemblies. *J. Phys. Chem.* **100**, 13323–13329 (1996).
- Alivisatos, A. P. Semiconductor clusters, nanocrystals and quantum dots. *Science* **271**, 933–937 (1996).
- Avouris, P. (ed.) *Atomic and Nanometer-Scale Modification of Materials: Fundamentals and Applications* (Kluwer, Dordrecht, 1993).
- Landman, U., Luedtke, W. D., Burnham, N. & Colton, R. J. Atomistic mechanisms and dynamics of adhesion, nanoindentation and fracture. *Science* **248**, 454–461 (1990).
- Bogachek, E. N., Zagoskin, A. M. & Kulik, I. O. Conductance jumps and magnetic flux quantization in ballistic point contacts. *Sov. J. Low Temp. Phys.* **16**, 796–800 (1990); *Fiz. Nizk. Temp.* **16**, 1404–1411 (1990).
- Pascual, J. I. *et al.* Quantum contact in gold nanostructures by scanning-tunneling microscopy. *Phys. Rev. Lett.* **71**, 1852–1855 (1993).
- Olesen, L. *et al.* Quantized conductance in an atom-sized point contact. *Phys. Rev. Lett.* **72**, 2251–2254 (1994).
- Pascual, J. I. *et al.* Properties of metallic nanowires: from conductance quantization to localization. *Science* **267**, 1793–1795 (1995).
- Krans, J. M., van Ruitenbeek, J. M., Fisun, V. V., Yanson, I. K. & de Jongh, L. J. The signature of conductance quantization in metallic point contacts. *Nature* **375**, 767–769 (1995).
- Smith, D. P. E. Quantum point contact switches. *Science* **269**, 371–373 (1995).
- Bratkovsky, A. M., Sutton, A. P. & Todorov, T. N. Conditions for conductance quantization in realistic models of atomic-scale metallic contacts. *Phys. Rev. B* **52**, 5036–5051 (1995).
- Costra-Kramer, J. L., Garcia, N., Garcia-Mochales, P. & Serena, P. A. Nanowire formation in macroscopic metallic contacts: quantum mechanical conductance tapping a table top. *Surface Sci.* **342**, 11144–11449 (1995).
- Lang, N. D. Resistance of atomic wires. *Phys. Rev. B* **52**, 5335–5342 (1995).
- Garcia-Martin, A., Torres, J. A. & Saenz, J. J. Finite size corrections to the conductance of ballistic wires. *Phys. Rev. B* **54**, 13448–13451 (1996).
- Rubio, G., Agrait, N. & Vieira, S. Atomic-sized metallic contacts; mechanical properties and electronic transport. *Phys. Rev. Lett.* **76**, 2302–2305 (1996).
- Scherbakov, A. G., Bogachek, E. N. & Landman, U. Quantum electronic transport through three-dimensional microconstrictions with variable shapes. *Phys. Rev. B* **53**, 4054–4064 (1996).
- Bogachek, E. N., Scherbakov, A. G. & Landman, U. Magnetic switching and thermal enhancement of quantum transport through nanowires. *Phys. Rev. B* **53**, R13246–R13249 (1996).
- Landman, U., Luedtke, W. D., Salisbury, B. E. & Whetten, R. L. Reversible manipulations of room temperature mechanical and quantum transport properties in nanowire junctions. *Phys. Rev. Lett.* **77**, 1362–1365 (1996).
- Landman, U., Luedtke, W. D. & Gao, J. Atomic-scale issues in tribology: interfacial junctions and nano-elastohydrodynamics. *Langmuir* **12**, 4514–4528 (1996).
- Stalder, A. & Durig, U. Study of yielding mechanics in nanometer-sized Au contacts. *Appl. Phys. Lett.* **68**, 637–639 (1996).

22. Landman, U., Barnett, R. N. & Luedtke, W. D. Nanowires: size evolution reversibility and one-atom contacts. *Z. Physik D* (in the press).
23. de Heer, W. A. The physics of simple metal clusters: experimental aspects and simple models. *Rev. Mod. Phys.* **65**, 611–675 (1993).
24. Martin, T. P. (ed.) *Large Clusters of Atoms and Molecules* (Kluwer, Dordrecht, 1996).
25. Yannouleas, C. & Landman, U. in *Large Clusters of Atoms and Molecules* (ed. Martin, T. P.) 131–200 (Kluwer, Dordrecht, 1996).
26. Barnett, R. N. & Landman, U. Born-Oppenheimer molecular-dynamics simulations of finite systems: structure and dynamics of (H₂O)₂. *Phys. Rev. B* **48**, 2081–2097 (1993).
27. Haberland, H. (ed.) *Clusters of Atoms and Molecules* (Springer Ser. in Chem. Phys. 52 & 57, Springer, Berlin, 1994).
28. Troulier, N. & Martin, J. L. Efficient pseudopotentials for plane-wave calculations. *Phys. Rev. B* **43**, 1993–2006 (1991).
29. Thouless, D. J. & Kirpartrick, S. Conductivity of the disordered linear chain. *J. Phys. C* **14**, 235–245 (1981).
30. Imry, Y. & Shiren, N. Energy averaging and the flux-periodic phenomena in small normal-metal rings. *Phys. Rev. B* **33**, 7992–7997 (1986).
31. Flyvbjerg, H. & Petersen, H. G. Error estimates on averages of correlated data. *J. Chem. Phys.* **91**, 461–466 (1989).
32. Bogachev, E. N., Scherbakov, A. G. & Landman, U. Shape-effects on conductance quantization in three-dimensional nanowires: hard versus soft potentials. *Phys. Rev. B* (in the press).

Acknowledgements. Calculations were performed at the National Energy Research Scientific Computing Center, Lawrence Berkeley, CA, and the GIT Center for Computational Materials Science. This work was supported by the DOE and AFOSR.

Correspondence should be addressed to U.L. (e-mail: uzi.landman@physics.gatech.edu).

Hollow nanoparticles of WS₂ as potential solid-state lubricants

L. Rapoport*, Yu. Bilik*, Y. Feldman†, M. Homyonfer†, S. R. Cohen‡ & R. Tenne†

* Department of Mechanics and Control, Center for Technological Education-Holon, PO Box 305, Holon 58102, Israel

† Department of Materials and Interfaces, ‡ Chemical Services Unit, Weizmann Institute, Rehovot 76100, Israel

Solid lubricants fill a special niche in reducing wear in situations where the use of liquid lubricants is either impractical or inadequate, such as in vacuum, space technology or automotive transport. Metal dichalcogenides MX₂ (where M is, for instance, Mo or W and X is S or Se) are widely used as solid lubricants. These materials are characterized by a layered structure with weak (van der Waals) inter-layer forces that allow easy, low-strength shearing^{1,2}. Within the past few years, hollow nanoparticles (HNs) of MX₂ with structures similar to those of nested carbon fullerenes and nanotubes have been synthesized^{3,4}. Here we show that these materials can act as effective solid lubricants: HN-WS₂ outperforms the solid lubricants 2H-MoS₂ and 2H-WS₂ in every respect (friction, wear and lifetime of the lubricant) under varied test conditions. We attribute the outstanding performance of HN-WS₂ to its chemical inertness and the hollow cage structure, which imparts elasticity and allows the particles to roll rather than to slide.

The material used in this study was synthesized by a solid-gas reaction⁵ which yields gram quantities of HN-WS₂, with limited control over the size distribution and shape of the nanoparticles. The average particle size of the 2H-WS₂ and 2H-MoS₂ powders was 4 μm; the average particle size of HN-WS₂ was 120 nm. Samples of the 2H-MoS₂ and 2H-WS₂ powders were milled for 24 hours, leading to platelets with an average size of 0.5 μm. Figure 1 shows schematic illustrations of the two main experimental set-ups which were used in the present work to evaluate the tribological properties of HN-WS₂ in comparison to bulk 2H-WS₂ (and 2H-MoS₂) powder. Using the disk-block tester at high sliding speeds and low loads (experiment A in Table 1), the rolling friction efficacy of HN-WS₂ can be examined. At high loads and lower velocities, the disk-block tester (experiments B and C in Table 1) probes the compliance of the HN films under conditions where mechanical effects dominate.

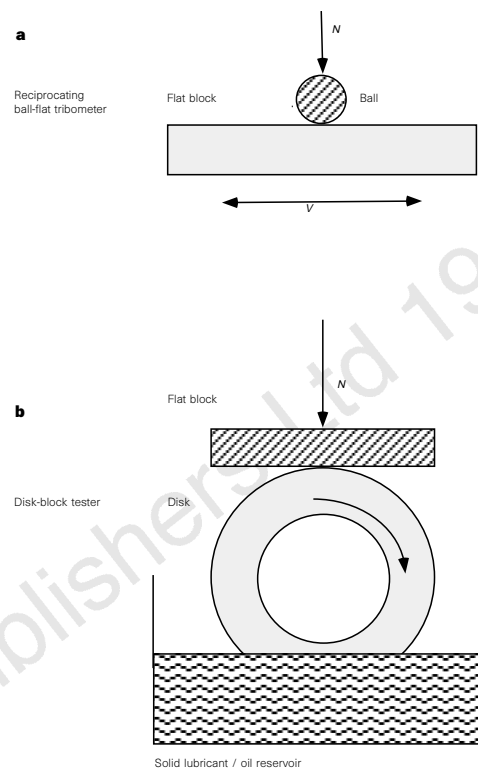


Figure 1 Diagrams of the two experimental set-ups which were used in the present work to investigate the tribological properties of HN-WS₂ and 2H-WS₂ (2H-MoS₂). **a**, Ball-flat tribometer: here, friction and wear of the various lubricants were investigated under low sliding velocities and loads. The load (*N*) and velocity (*V*) of the flat were varied in a predetermined manner and the friction coefficient (slope of friction versus load) was determined. The size of the wear track and the ball surface were examined after each run with an optical microscope. Quantitative analysis of the wear tracks with scanning force microscope (SFM) was undertaken. To test the solid lubricants under more realistic conditions (larger loads and velocities), the disk-block tester **b** was employed.

Figure 2 shows the results of the wear measurements using the tribometer. Wear volumes were determined from the depth and width of the wear track. Wear volumes of 2H-MoS₂ both dry and wetted with a drop of oil, were 6.5 and 2 times that of HN-WS₂, respectively. The wear for pure mineral oil is 65 times greater. These results (supported by other data; see Supplementary Information) confirm the visual impression of Fig. 2, namely that the wear track produced by the wall when HN-WS₂ powder was used, was the smallest of all solid lubricants examined. Although the ball surface was under continuous load during the entire test, each segment of the flat block experienced only instantaneous load as the ball slid over it. Therefore the ball surface suffered most of the thermal stress, which is shown by the large difference in its wear among the different powders (Fig. 2). Here again, the amount of wear for the HN-WS₂ powder was smallest.

In Table 1 we show the results of an experiment in which rolling of the particles is allowed, because of high speeds and low loads (experiment A). To simulate typical industrial conditions, only 5 wt% solid lubricant, in a commercial oil, was used. We note that friction (μ) and wear (w) coefficients, and also the average surface roughness (R_a), were smallest for the HNs (see also Supplementary Information). In experiments B and especially, experiment C (Table 1) the compressive regime is accessed. Obviously, the wear of the HN-WS₂/oil mixture was the smallest of the three, which demonstrates again the superior wear protection of the nano-material compared with the 2H counterparts. It is also clear that